Journal of
Applied Remote Sensing

Use of MODIS 16-day albedos in generating GOES-R advanced baseline imager imagery

Lewis Grasso
Donald W. Hillger
Crystal Barker Schaaf
Zhuosen Wang
Renate Brummer
Robert DeMaria

Use of MODIS 16-day albedos in generating GOES-R advanced baseline imager imagery

Lewis Grasso,[a] Donald W. Hillger,[b] Crystal Barker Schaaf,[c] Zhuosen Wang,[c] Renate Brummer,[a] and Robert DeMaria[a]

[a]Colorado State University, Cooperative Institute for Research in the Atmosphere, CIRA – 1375, Fort Collins, Colorado 80523-1375

Lewis.Grasso@colostate.edu

[b]Colorado State University, NOAA/NESDIS/STAR/RAMMB, CIRA – 1375, Fort Collins, Colorado 80523-1375

[c]University of Massachusetts, Environmental Earth and Ocean Sciences, Boston, Massachusetts 02125

Abstract. Advanced preparation for satellite data from the next-generation GOES-R advanced baseline imager (ABI) is supported by coupling high resolution mesoscale and radiative transfer numerical models. Calculated GOES-R ABI imagery is produced in a two-step process. First, a mesoscale model is used to simulate an event over a region with 400 m horizontal grid spacings; secondly, output from the mesoscale model is used as input to a second model that calculates top of the atmosphere radiances at selected GOES-R ABI wavelengths. Such radiances or brightness temperatures are referred to as synthetic imagery. In order for the synthetic imagery to contain realistic horizontal variability of values of surface reflectance at wavelengths from 0.44 to 2.25 μm, MODIS 16-day albedos are incorporated in the radiative transfer calculations. One application of synthetic GOES-R imagery is that of algorithm development and testing. Algorithms may focus on, but are not limited to, the detection and retrieval of smoke, volcanic ash, fires, blowing dust, and the state of surface physiography. Proper identification of such features is, at times, dependent on the horizontal variability of surface reflectance values. MODIS 16-day spectrally dependent albedos are a valuable dataset in aiding the generation of synthetic GOES-R imagery. [DOI: 10.1117/1.JRS.7.073584]

Keywords: MODIS; albedo; GOES-R; advanced baseline imager; fire; volcanic ash; synthetic imagery.

Paper 12210 received Jul. 16, 2012; revised manuscript received Dec. 18, 2012; accepted for publication Jan. 24, 2013; published online Feb. 22, 2013.

1 Introduction

For the past several years, synthetic GOES-R advanced baseline imager (ABI) imagery has been produced at the Cooperative Institute for Research in the Atmosphere (CIRA). A few reasons exist to motivate this effort. First, synthetic imagery can help with the interpretation of observed imagery; second, to prepare for future sensors such as the ABI that will be on the GOES-R satellite; and third, to help evaluate solutions from numerical models.[1] Although the imagery of future satellites can also be generated from observed satellite imagery,[2] synthetic imagery has a few advantages. Temporal sampling from ABI will be 5 min with a footprint size of at most 2 km.[3] Satellites currently in geostationary orbit may at times be able to produce imagery at a frequency similar to ABI, but not the footprint size. In contrast, satellites in polar orbit may be able to produce a footprint similar to ABI, but not replicate the temporal frequency. With synthetic imagery, both the temporal frequency and footprint size similar to those of ABI can be generated.

0091-3286/2013/$25.00 © 2013 SPIE

One of the first steps in developing a system to produce synthetic satellite data is to generate synthetic imagery of operational satellites and make a direct comparison with observations. Grasso et al.[1] compared synthetic GOES-12 to observed GOES-12 at both 6.5 and 10.7 μm for a thunderstorm event that occurred on 8 May 2003. Results indicated that the synthetic imagery was in reasonable agreement with observed imagery at both wavelengths. A relatively small cold bias, on the order of a few Kelvins, was noted at the tops of thunderstorms. Similar to efforts at CIRA, synthetic imagery is also being produced at the Cooperative Institute for Meteorological Satellite Studies (CIMSS). Otkin et al.[4] conducted a large scale simulation and compared synthetic Spinning Enhanced Visible and Infrared Imager (SEVIRI) to observed SEVIRI at seven infrared bands. Results showed reasonable agreement between observed and synthetic SEVIRI imagery. In addition to the separate SEVIRI bands, the channel differences of synthetic imagery also compared well with observed channel differences. As a result of the above studies, both CIMSS and CIRA have been producing datasets of synthetic GOES-R imagery for the purpose of aiding the development and testing of a variety of ABI detection and retrieval algorithms. In addition to algorithm development, synthetic imagery can also be used to evaluate numerical models.

Numerical models are typically evaluated by comparing certain predicted variables with observations. Some of these variables include surface winds, temperatures, dewpoint temperatures, and pressure. Upper air data is also used to compare simulated variables on constant pressure surfaces. Simulated clouds, on the other hand, are a challenge to evaluate. Synthetic imagery is an ideal way to compare simulated clouds directly to observed cloud fields. In one case, Grasso and Lindsey[5] compared synthetic GOES-12 imagery at 3.9 μm to observed imagery and found a discrepancy between two simulated thunderstorm anvils over the upper Midwest. Observed GOES-12 imagery indicated that the simulated thunderstorms reflected less solar energy compared to observed thunderstorms. This result suggested an error with the prognostic equation of pristine ice number concentrations. Once the error was fixed, the resulting synthetic imagery was in accord with observations. In another study, Jankov et al.[6] simulated an atmospheric river event over California. Several simulations were performed with the Weather Research and Forecasting-Advanced Research WRF (WRF-ARW) model[7]; the only difference between the runs was the choice of microphysics. Synthetic GOES-10 imagery was produced at 10.7 μm and compared to observed GOES-10 imagery for each of the microphysical runs. Results were able to identify strengths and weaknesses of the microphysical schemes. The above two examples illustrate the value of using synthetic imagery to evaluate the solution of a numerical model.

One feature common to synthetic imagery at wavelengths greater than or equal to 3.9 μm is the inclusion of spectrally dependent surface emissivity values. Satellite-based surface emissivity values[8] are a robust way to include surface heterogeneity in synthetic imagery. An examination of the solar and terrestrial Planck functions indicates that both curves intersect near 3.9 μm. At this and longer wavelengths, the Earth emits energy; hence, the use of spectrally dependent surface emissivity values when making synthetic imagery. In contrast, however, the Earth emits little energy at wavelengths shorter than 3.9 μm; rather, the surface of the Earth reflects incoming solar energy. As a result, surface emissivity values should be replaced with spectrally dependent surface albedo values when producing synthetic imagery at wavelengths less than 3.9 μm. In this study, similar to surface emissivity values, surface albedo values are based on measurements from the moderate-resolution imaging spectroradiometer (MODIS) instrument and are referred to as MODIS 16-day albedos.[9,10]

GOES-R ABI will have six bands, or channels, with central wavelengths less than 3.9 μm. They are 0.47, 0.64, 0.867, 1.38, 1.61, and 2.25 μm. In particular, 0.47 and 0.64 μm are designated as the blue and red bands, respectively. ABI is void of a green band near 0.55 μm; one consequence is the challenge of producing a natural color image from the combination of the red, green, and blue bands. In spite of this shortfall, methods are being explored at CIRA to produce natural color imagery from ABI by using the near infrared band at 0.867 μm. This method employs look-up tables to construct a green band from the channels centered at 0.47, 0.64, and 0.867 μm.[11,12] Once a green band is derived, an ABI natural color image can be produced.

Details of the process of generating synthetic ABI imagery at wavelengths that contain solar reflection is described herein. Different examples of synthetic ABI imagery utilizing

MODIS 16-day albedos are included. They encompass natural color imagery of cloudy scenes, the inclusion of an idealized volcanic ash and smoke plume, and hotspots from canopy wildfires. Realistic synthetic ABI imagery has potential uses in the development and testing of detection and retrieval algorithms.

2 Computational Methodology

Two numerical models were used to simulate past weather events. They are the Colorado State University Regional Atmospheric Modeling System (CSU-RAMS) model[13] and the WRF-ARW model.[7] Both models simulated variables on four grids. Grid 1, spanning the largest area, had horizontal grid spacings of 50 km in each direction; grid 2, had horizontal grid spacings of 10 km; while grids 3 and 4 had horizontal grid spacings of 2 km and 400 m, respectively. A value of 2 km was chosen for grid 3 as this value is near the size of the GOES-R ABI footprint. On the other hand, 400 m was chosen to allow the inclusion of subpixel fire hotspots in the post-simulated domain of grid 4. Grids 2 through 4 were nested within their respective parent grid; all grids employed two-way interactive communication of prognostic variables. An illustration of the sizes of all four grids is displayed in Fig. 1. In all cases, two-moment microphysics was chosen. RAMS simulations included the small and large cloud droplet hydrometeor class along with pristine ice, snow, aggregates, hail, graupel, and rain water. In all eight hydrometeor classes, both the mass mixing ratio and number concentrations were predicted. WRF-ARW simulations included the following hydrometeor classes: cloud droplets, rain water, ice, snow, and graupel. In contrast to RAMS, all hydrometeor mass mixing ratio and number concentrations were predicted except for cloud droplets. Two-moment microphysics was chosen due to the important dependence of the reflection of solar energy on particle size.

Depending on the simulation, model initialization used the North American Regional Reanalysis dataset[14] or data from the Global Forecast System.[15] All simulations were run for a total of at least 6 h while output was written at a frequency of 5 min. This value was chosen to match the temporal sampling frequency of the ABI instrument. After a simulation completed, output was then used as input to another model that computed ABI top of the atmosphere radiances.

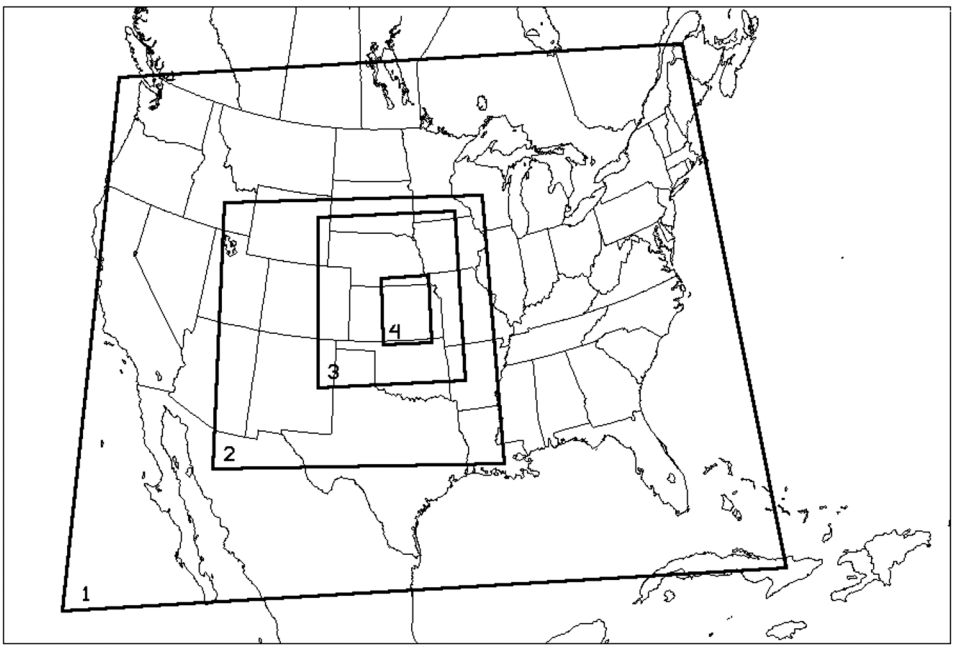

Fig. 1 An illustrative example of the relative sizes of the four grids used in simulations with RAMS and WRF-ARW. Although the actual location of the grids depends on the particular event being simulated, the sizes of each grid remained fixed.

Radiance calculations were performed by an observational operator that was developed at CIRA.[16–18] Radiance values at 0.47, 0.64, 0.865, and 2.25 μm were calculated using a one-dimensional version of the spherical harmonic discrete ordinate method (SHDOMPP).[19] In general, absorption by water vapor should be included in radiance calculations for some of the ABI bands. At the bands listed above, however, absorption by water vapor is less important than Raleigh scattering; as a result, water vapor absorption was neglected. Cloud hydrometeor optical properties (total extinction and single-scattering albedo) were calculated from modified anomalous diffraction theory.[20] Also at the wavelengths listed above, SHDOMPP requires surface albedos as a lower boundary condition. Horizontally varying values of surface albedo were chosen over a horizontally constant value. As a result, MODIS derived values of surface albedo were used.

The MODIS bidirectional reflectance distribution function (BRDF) and albedo standard product (MCD43) is produced globally on a 500 m grid.[9,10,21,22] A semi-empirical BRDF model is fit to all high-quality, cloud-clear, atmospherically corrected, directional surface reflectances available over a 16-day period. Data from MODIS instruments on both the Terra and Aqua satellites are used. High-quality spectral retrievals are only possible when there are sufficient directional observations to adequately sample the surface reflectance anisotropy. These BRDFs are then integrated over all view and illumination angles to generate bihemispherical reflectances (or white sky albedos) under isotropic illumination. The validated[23–26] white sky quantity is an intrinsic measure of the surface albedo and does not include atmospheric multiple scattering effects. However, white sky values are used here as a stable representation of the reflective character and variability of the surface for the purpose of generating synthetic GOES-R ABI radiances.

3 Development of Natural Color GOES-R ABI Imagery

Two existing simulated case studies were used to aid in the development of natural color imagery for the ABI sensor. These are the 23 October 2007 southern California wildfire event and the 27 June 2005 upper Midwest convective event. The first case study was simulated to aid in the development of a GOES-R fire retrieval algorithm. This was done by producing synthetic ABI imagery at 2.25, 3.9, 10.35, and 11.2 μm. During the day on 27 June 2005, a cold front had moved southward over the northern central plains of the United States. One consequence was the development of thunderstorms over eastern Wyoming and central Iowa. Once the thunderstorms produced an anvil canopy, observed GOES-12 imagery at 3.9 μm indicated a relatively significant difference in the reflective signature over the majority of the anvils of these thunderstorms. Due to the different behavior of the anvils, this case was simulated with RAMS to study the possible different microphysical structure of the anvils.[5] As a result of the computational demands of these simulations, both cases were chosen to be used to aid in the development of synthetic natural color GOES-R imagery.

Since a green band is absent from the ABI instrument, reflectance values for green [Refl(G)] are derived from the following three ABI bands: blue (B: 0.47 μm), red (R: 0.64 μm), and near infrared (NIR: 0.865 μm). This is done using the following regression formula:

$$\mathrm{Refl}(G) = 0.416 * \mathrm{Refl}(R) + 0.523 * \mathrm{Refl}(B) + 0.065 * \mathrm{Refl}(\mathrm{NIR}) - 0.005. \quad (1)$$

Once a green band has been acquired, a natural color image is produced by combining the blue, green, and red bands. In addition, effects of Rayleigh scattering have been minimized in the natural color image followed by the application of an enhancement that is designed to brighten the image.[11,12] In order to obtain realistic horizontal variability in surface reflectance, MODIS-derived albedo values were used as a lower boundary condition to SHDOMPP in both cases. Although albedo values are only retrieved over land, albedo values did exists over some inland water bodies,such as the Salton Sea over southern California. These spectrally dependent values were used for portions of the Pacific Ocean west of California. One possible alternative to utilizing the MODIS derived albedo values would be to use a constant value over the domain. The resulting image, however, would appear unrealistic.

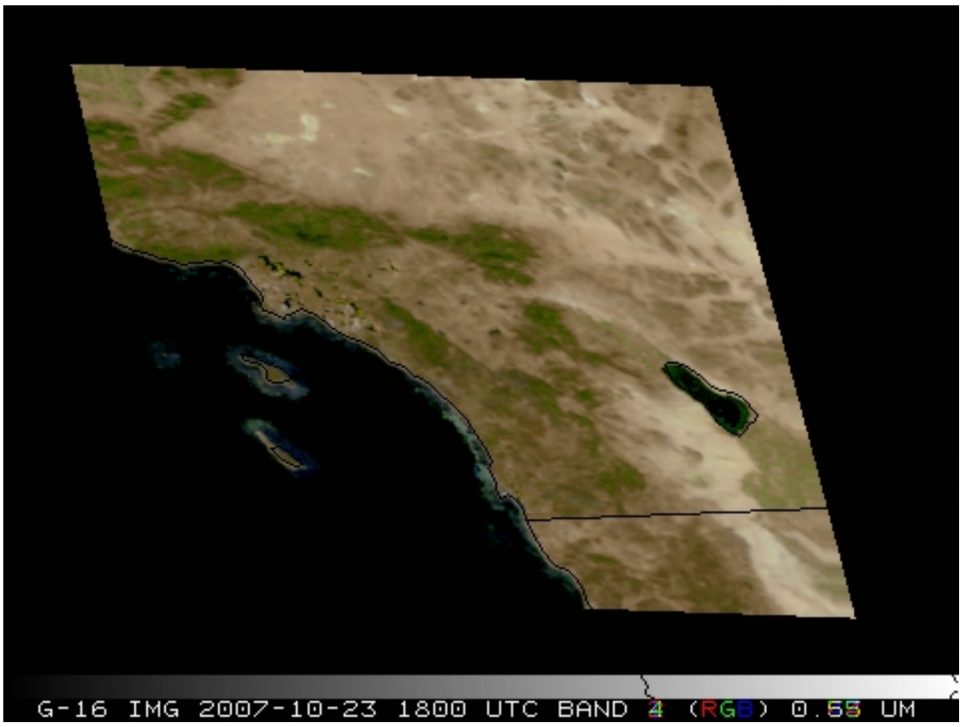

Fig. 2 Natural color image of the cloud-free 23 October 2007 southern California case, at 1800 UTC, using a look-up table green reflectance values from Eq. (1).

The above procedure was first applied to the 23 October 2007 southern California wildfire case, at 1800 UTC, neglecting any clouds that may have formed during the simulation (Fig. 2). One way to evaluate the natural color image generated with a green band derived from Eq. (1) is to generate a synthetic green band at 0.555 μm from SHDOMPP (Fig. 3). As can be seen in the figures, the natural color image in Fig. 2 has a green bias. This may be a consequence of the number of observed satellite images used to build the coefficients in Eq. (1). Since the simulation of the southern California case produced few clouds, the 27 June 2005 case was used to make synthetic natural color imagery that includes clouds.

As stated above, SHDOMPP is a one-dimensional radiative transfer model. That is, radiance values are computed along one atmospheric column and they are independent of adjacent columns. Therefore, variability in the values of reflectivity at cloud top is a consequence of variations in cloud optical depth as opposed to cloud shadows. For the 27 June 2005 case, imagery was generated every 5 min, to match the sampling rate of ABI, over a 6-h period from 1800 UTC 28 June 2007 to 0000 UTC 29 June 2007. In addition, the time dependence of incoming solar radiation was accounted for over the 6-h period that imagery was produced. A loop showing the final product, using derived green reflectance values from Eq. (1), is displayed in Video 1. Both cases were then extended with the inclusion of (1) an idealized smoke plume for the 23 October 2007 case and (2) an idealized volcanic ash plume for the 27 June 2005 study.

3.1 *Inclusion of an Idealized Smoke and Volcanic Ash Plume*

As a first step at producing synthetic GOES-R natural color imagery that contains an aerosol, an idealized smoke plume was included in the radiative transfer calculations of the 23 October 2007 study. Natural color MODIS imagery of this event (Terra pass, 1825 UTC, 23 October 2007) was used to extract information about the shape and display-screen brightness of the observed smoke plume. Brightness values varied from 0.0 to 1.0. Values of the optical properties (extinction, single-scatter albedo, and asymmetry factor) of the smoke plume were adapted from Reid et al.[27] Optical properties of the plume were specified within a layer that extended from 1 to 3 km above the ground and were vertically constant. Spectrally dependent extinction values

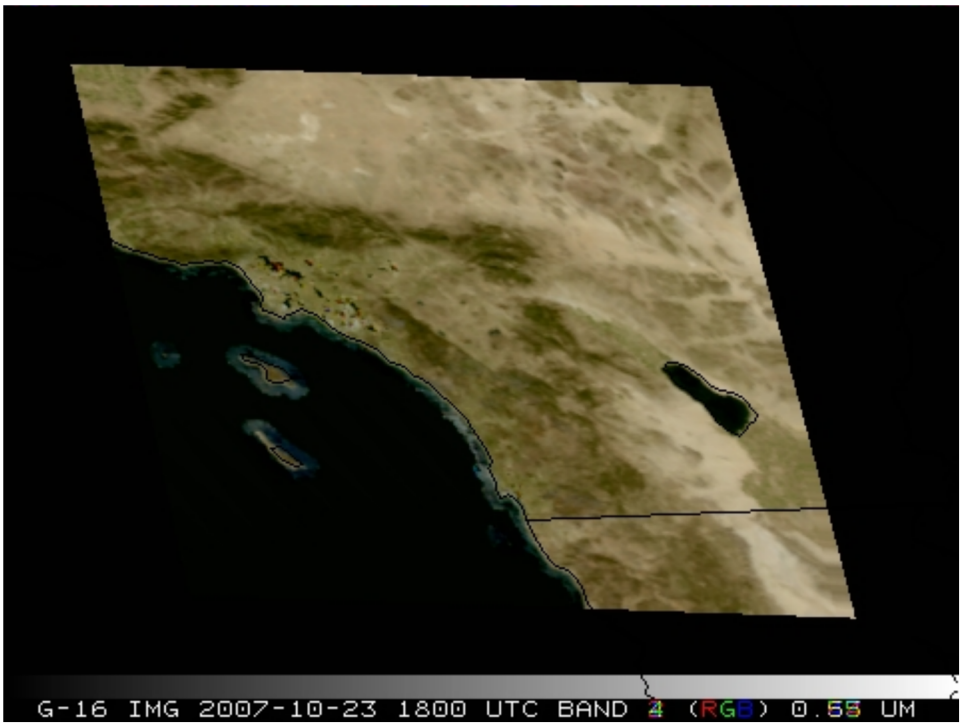

Fig. 3 Natural color image of the cloud-free 23 October 2007 southern California case, at 1800 UTC, using synthetic green reflectance values from SHDOMPP.

were multiplied by the extracted brightness of the observed plume. This was done to produce some horizontal structure within the smoke plume of the synthetic GOES-R natural color image. Reflectance values of each synthetic band were produced and compared to observed reflectance values at the corresponding MODIS band. Such a comparison was done to assure that the synthetic reflectance values from the smoke plume compared reasonable well to observed values. Once this was accomplished, a natural color synthetic ABI image was produced (Fig. 4). As can been seen in the figure, most of the smoke plume existed over water. In order to include an aerosol over land, an idealized volcanic ash plume was included in the 27 June 2005 study.

Similar to the smoke plume in the 23 October 2007 case, MODIS imagery of the Eyjafjallajökull eruption (Terra pass, 12:40 UTC, 7 May 2010) that extended southward from southern Iceland was used. Information about the shape and brightness of the ash

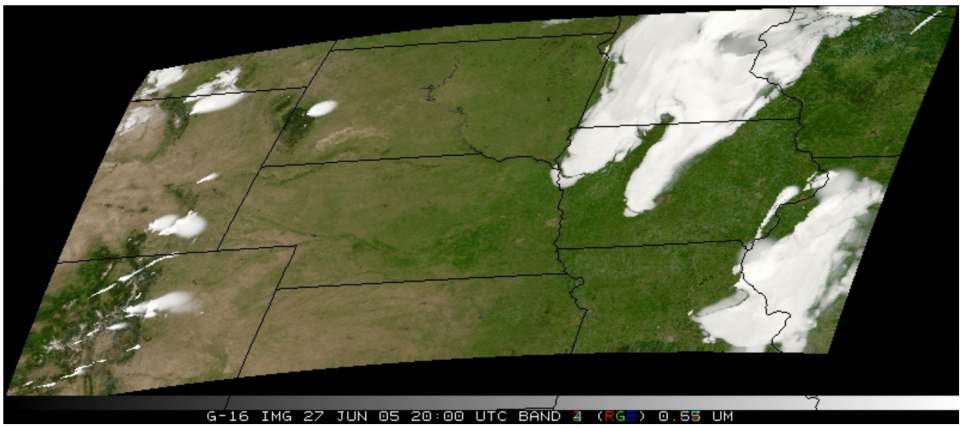

Video 1 Natural color loop from 1800 UTC 27 June 2005 to 0000 UTC 28 June 2005 over the northern central plains of the U.S. (MOV, 3.5 MB) [URL: http://dx.doi.org/10.1117/1.JARS.7.1.073584.1].

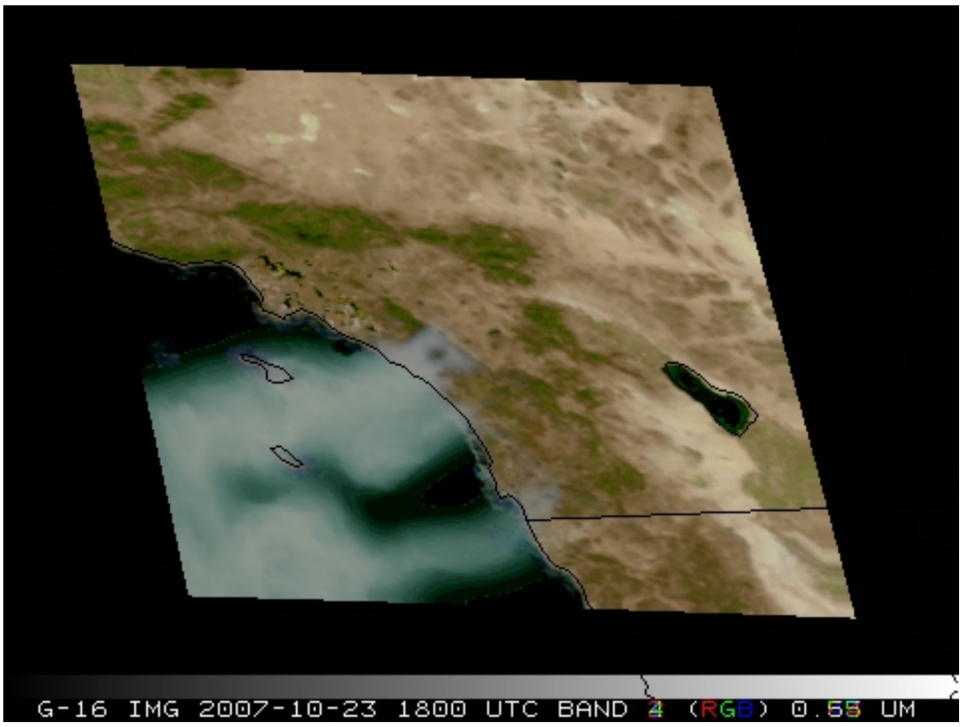

Fig. 4 Same as Fig. 2 with an idealized smoke.

plume was extracted from the imagery. This particular MODIS image was chosen because of the northwest to southeast orientation of the plume. Brightness values for this case also varied from 0.0 to 1.0. Values of optical properties (extinction, single-scatter albedo, and asymmetry factor) of the ash plume were adapted from Prata and Grant.[28] Values of the extinction were multiplied by the extracted brightness of the plume in the MODIS image. The plume was placed between 8 and 11 km above ground and was vertically homogeneous. Synthetic ABI reflectance values at 0.47, 0.64, and 0.865 μm were compared to observed MODIS reflectance values. After synthetic reflectance values compared favorably to observed values, a natural color image was produced (Fig. 5). For clarity, reflectance values for green in Fig. 5 were derived from Eq. (1).

Unlike the smoke plume in Fig. 4, the ash plume in Fig. 5 exhibits a color that is similar to some clear-sky regions. In particular, the color of the ash is similar to portions of the surface of Wyoming and eastern Colorado. Since some ash retrieval methods may rely on background values of surface albedo, a preliminary test of the sensitivity of the color of the ash to variations

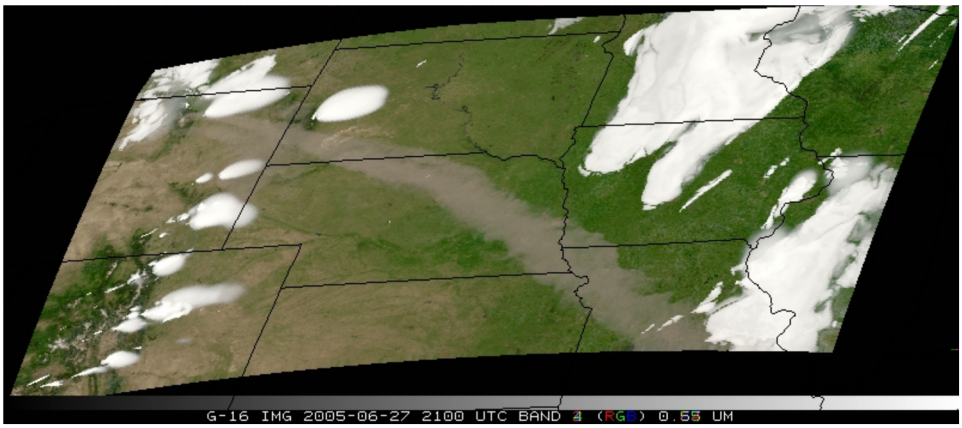

Fig. 5 Synthetic GOES-R ABI natural color image of an idealized volcanic ash plume included in the 27 June 2005 study.

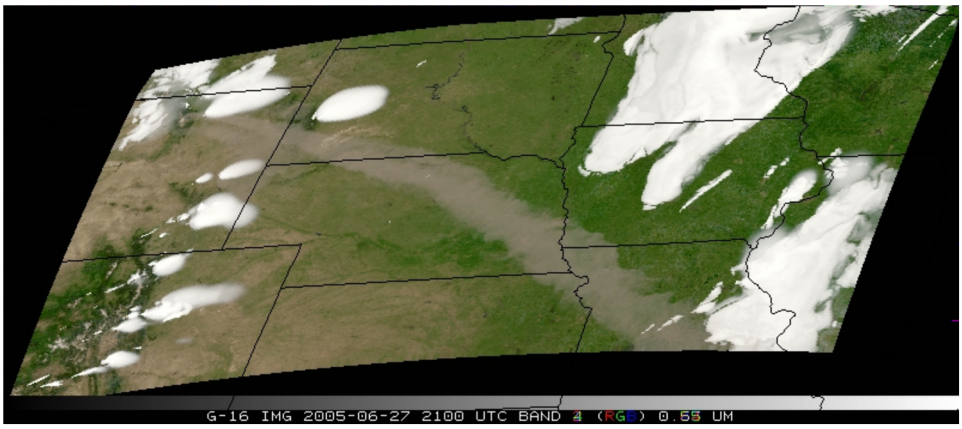

Fig. 6 Same as Fig. 5 except the reflectance values of the ash plume were increased by 10% at 0.865 μm.

in values of the radiance at 0.865 μm band was examined. The coefficient of the NIR band in Eq. (1), 0.065, is approximately one order of magnitude smaller that of the other two coefficients. This suggests that some uncertainty in the value of the radiances at 0.865 μm may have a relatively small impact on the values of radiances for the derived green band, and thus the natural color of the ash. Values of the single-scatter albedo were increased, only for the ash, at 0.865 μm until reflectance values of the ash were about 10% larger than those used to generate Fig. 5. The corresponding green band was derived and the subsequent natural color image was generated (Fig. 6). Likewise, the procedure was repeated, but this time until the reflectance values of the ash were about 10% lower than those used to generate Fig. 5. After the green band was derived, the natural color image was generated (Fig. 7).

In order to highlight the difference of the values of reflectivity in the derived green band, differences were calculated. This was done by computing the following formulas:

$$\text{Percent change} = 100.0 * [\text{IncRefl}(G) - \text{Refl}(G)]/\text{IncRefl}(G) \tag{2}$$

$$\text{Percent change} = 100.0 * [\text{DecRefl}(G) - \text{Refl}(G)]/\text{DecRefl}(G) \tag{3}$$

where $\text{IncRefl}(G)$ and $\text{DecRefl}(G)$ are the values of reflectivity of the derived green band using the 0.865 band with increased and decreased reflectivity values of the ash, respectively. Results from Eq. (2) are shown in Fig. 8 and indicate an approximate 2.5 percent increase in the derived green reflectance values. Similarly, results from Eq. (3) are shown in Fig. 9 and indicate an

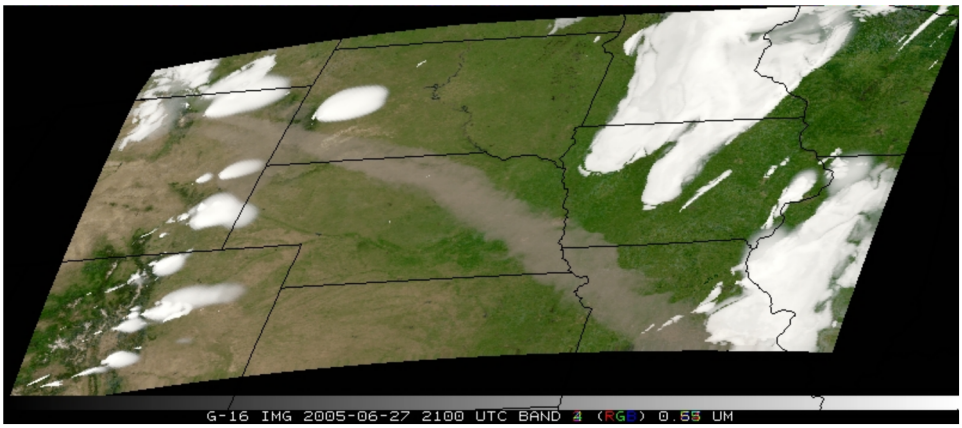

Fig. 7 Same as Fig. 5 except the reflectance values of the ash plume were decreased by 10% at 0.865 μm.

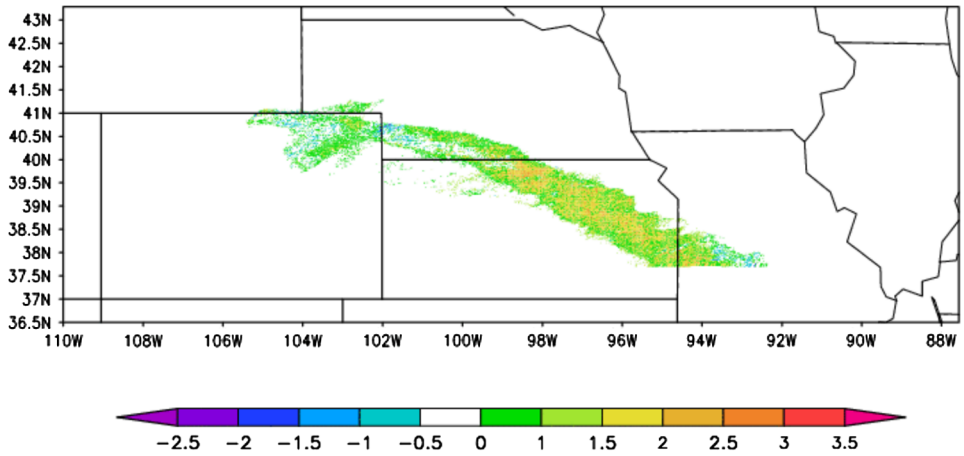

Fig. 8 Percent change in look-up table green reflectance values by using a 10 percent increase in the reflectance values of just the ash plume in the 0.865 bands.

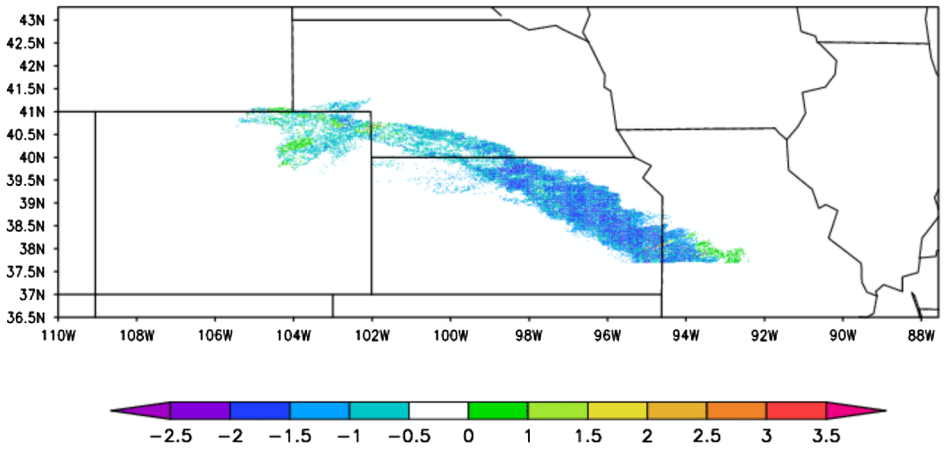

Fig. 9 Percent change in look-up table green reflectance values by using a 10 percent decrease in the reflectance values of just the ash plume in the 0.865 bands.

approximate 1.5 percent decrease. These results suggest that a rather significant error in measured 0.865 μm reflectance values will lead to a relatively small variation in derived green reflectance values using Eq. (1). However, note that the weights of Refl(R) and Refl(B) are approximately one order of magnitude larger than the weight of Refl(NIR). As a result, a larger constraint is placed on the accuracy of measured Refl(R) and Refl(B) relative to Refl(NIR).

3.2 *GOES-R ABI 2.25 μm Imagery of Fire Hotspots*

Operational GOES-13 and GOES-15 are capable of imaging subpixel hotspots from active fires at 3.9 μm. Common fire types are canopy wildfires, grassland fires, and agricultural fires. At times, some fires become either large and/or hot enough that the radiance measurements of the imager, for either satellite, saturate at 3.9 μm. For both satellites the saturation temperature of the imager at 3.9 μm is near 330 K. As a result, fire detection and retrieval algorithms are unable to retrieve fire information when the imager saturates at 3.9 μm. Retrieval of fire information is used as input to aerosol prediction systems. This information is then used for, but not limited to, visibility forecasting.[29]

In addition to fires causing the saturation of either imager, in the warm season in the United States relatively large skin temperatures of nonfire pixels can also saturate the imager at 3.9 μm. This typically occurs over southwestern portions of the U.S. and creates a challenge to retrieve

fire information from either GOES-13 or GOES-15. In recognition of the above issues, the ABI has a design so that imager saturation will occur at a larger temperature: approximately 400 K at 3.9 μm.

Due to the higher saturation temperature at 3.9 μm for the ABI instrument, a larger percentage of otherwise nonretrievable fires from GOES-13 and/or GOES-15 may become retrievable. Some canopy wildfire, however, may still cause saturation of the ABI at 3.9 μm; thus no information may be obtained from such fires. One difference between the ABI and the current imager on GOES-13 or GOES-15 is the inclusion of several additional channels. One such channel is centered near 2.25 μm.

Although one purpose of measurements at 2.25 μm is to infer information about cloud properties and cloud particle size, subpixel hotspots from active burning may also be present at this band. This was the motivation for producing synthetic 2.25 μm GOES-R ABI imagery that contains fire hotspots. Some subpixel hotspots may saturate the ABI at 3.9 μm and be hot enough to radiate enough energy at 2.25 μm to appear in imagery at this wavelength. Such a result suggests that although some fires may elude retrieval at 3.9 μm, radiant energy at 2.25 μm of subpixel fires may allow fire information to be obtained via retrieval at this wavelength.

Synthetic 2.25 μm GOES-R ABI imagery was produced for the 23 October 2007 wildfire case over southern California. Fire information was obtained from the Wild Fire-Agricultural Biomass Burning Algorithm (WF-ABBA).[30] Information extracted from this dataset was a satellite pixel temperature, latitude, longitude, and a variable indicating the confidence that the measured radiance was consistent with a fire. Each latitude longitude pair of a satellite pixel associated with a fire was used to locate the grid point in the simulated domain where the fire will be located. Satellite retrieved fire temperatures then replaced the simulated canopy temperature in the model domain. Finally, a two-dimensional field of simulated canopy temperatures (containing satellite retrieved fire temperatures) was passed into a radiative transfer model. This model then calculates values of the top of the atmosphere radiance at 2.25 μm. Due to the smallest horizontal grid spacings of 400 m, the smallest fire size was 400 m. Although such a size may be too large in some cases, this is a first step at including subpixel fires in synthetic ABI imagery. Since the surface of the Earth reflects solar energy at 2.25, use of the MODIS 16-day albedo product was essential to generate realistic synthetic imagery.

Inclusion of MODIS 16-day albedo values highlights the spatial dependence of the subpixel fire. That is, the appearance of fires at 2.25 μm will depend on the reflective nature of the nonburning surface that surrounds the fire. For a given fire, a relatively large contrast between the fire and the nonburning surface could exist. In contrast, the same fire in a different location may have a relatively small contrast with the nonburning surface. This would be due to the large reflective nature of the nonburning surface. Therefore, the use of MODIS 16-day albedo values is essential for the generation of realistic ABI imagery containing subpixel fires. These issues are demonstrated in Video 2.

4 Summary and Future Direction

Synthetic imagery, presented herein, was produced for the GOES-R ABI bands that contain radiances primarily from solar reflection from the surface of the Earth. One way to produce realistic imagery is through the inclusion of the MODIS 16-day albedo product. Without horizontally varying surface albedo data, all synthetic imagery of the solar bands for ABI would be unrealistic. A constant surface albedo could give the false impression that fire detection with synthetic imagery at 2.25 μm is less challenging compared to the same process with observed imagery. Dust detection is less challenging over water compared to over land; smoke detection can be challenging over a stratus cloud layer compared to the land surface. This example is far from hypothetical. In October 2012, the Fern Lake fire, located in Rocky Mountain National Park, produced a smoke plume that moved eastward. In time, the smoke plume moved above a stratus cloud layer that was over the Front Range of northern Colorado. These are a few example of how detection of a feature may depend on the varying characteristics of the background albedo.

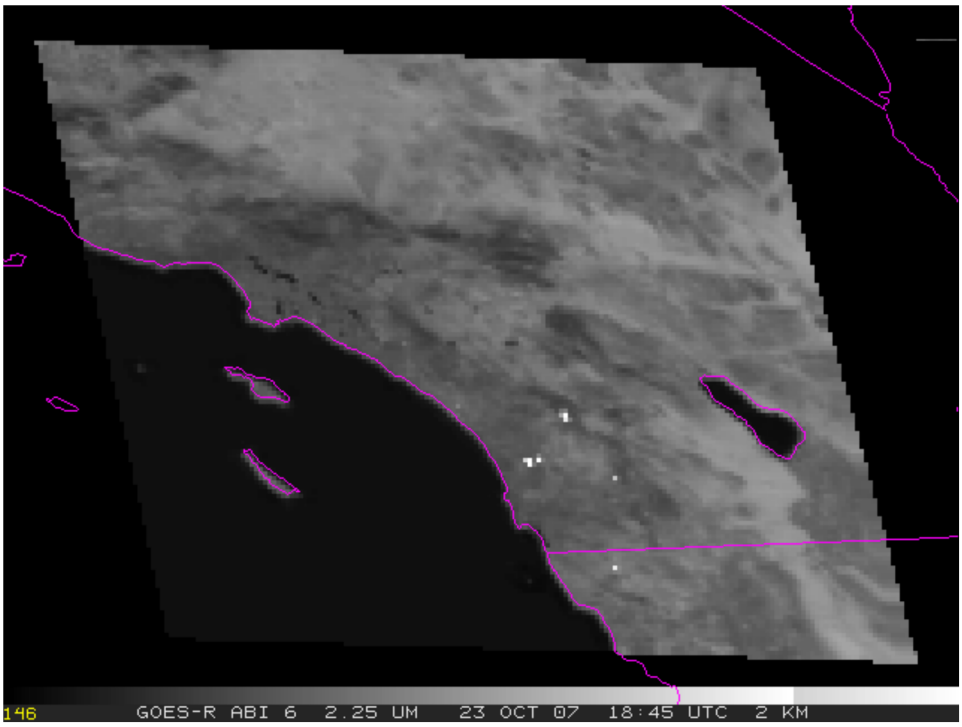

Video 2 Loop of synthetic GOES-R ABI subpixel fires (white pixels) at 2.25 μm from 1500 to 2055 UTC 23 October 2007 over southern California (MOV, 1.8 MB) [URL: http://dx.doi.org/10.1117/1.JARS.7.1.073584.2].

Although the ABI lacks a green band, natural color imagery can be produced from the blue band (0.47 μm), the red band (0.64 μm), and the near IR band (0.865 μm). Results presented herein suggest that derived green band reflectance values are less sensitive to errors in observed reflectance values at 0.865 μm compared to those at 0.47 and 0.64 μm. Examples of synthetic natural color imagery contained aerosols such as smoke, volcanic ash, and fire hotspots.

Synthetic satellite imagery represents an important component in the development and testing of detection and retrieval algorithms. Observations that can be used to evaluate detection and retrieval algorithms are, in general, lacking. Whereas optical properties are specified when synthetic imagery is made. This way, detection and retrieval algorithms can process synthetic imagery and compare retrieved properties, such as optical depth of volcanic ash, with those that were specified to make the imagery. Future work will focus on the generation of synthetic GOES-R ABI imagery containing a time-dependent smoke and dust plume. That synthetic imagery will then be available for the purpose of testing algorithms to detect and retrieve aerosol optical properties.

Acknowledgments

This research is primarily funded by NOAA's National Environmental Satellite, Data, and Information Service GOES-R Program Office. We thank Dr. Fred Prata of the Climate and Atmospheric Department, Norwegian Institute for Air Research, Kjeller, Norway for providing us with optical properties of volcanic ash plumes.

References

1. L. D. Grasso, M. Sengupta, and M. DeMaria, "Comparison between observed and synthetic 6.5 and 10.7 μm GOES-12 imagery of thunderstorms that occurred on 8 May 2003," *Int. J. Remote Sens.* **31**(3), 647–663 (2010), http://dx.doi.org/10.1080/01431160902894483.

2. S. D. Miller et al., "NexSat–Previewing NPOESS/VIIRS imagery capabilities," *Bull. Amer. Meteor. Soc.* **87**(4), 433–446 (2006), http://dx.doi.org/10.1175/BAMS-87-4-433.
3. T. J. Schmit et al., "Introducing the next-generation advanced baseline imager on GOESR," *Bull. Amer. Meteor. Soc.* **86**(8), 1079–1096 (2005), http://dx.doi.org/10.1175/BAMS-86-8-1079.
4. J. A. Otkin et al., "Validation of a large-scale high-resolution WRF model simulation using SEVIRI satellite observations," *J. Appl. Meteor. Climatol.* **48**(8), 1613–1626 (2009).
5. L. Grasso and D. Lindsey, "An example of the use of synthetic 3.9 μm GOES-12 imagery for two-moment microphysical evaluation," *Int. J. Remote Sens.* **32**(8), 2337–2350 (2011), http://dx.doi.org/10.1080/01431161003698294.
6. I. L. Jankov et al., "An evaluation of five WRF-ARW microphysics schemes using synthetic GOES imagery for an atmospheric river event affecting the California coast," *J. Hydrometeorol.* **12**(4), 618–633 (2011), http://dx.doi.org/10.1175/2010JHM1282.1.
7. W. C. Skamarock et al., "A description of the advanced research WRF version 2," NCAR Tech. Note/TN-468+STR, p. 88 (2005).
8. S. W. Seeman et al., "Development of a global infrared land surface emissivity database for application to clear sky sounding retrievals from multispectral satellite radiance measurements," *J. Appl. Meteor. Climatol.* **47**(1), 108–123 (2008).
9. C. B. Schaaf et al., "First operational BRDF, albedo and nadir reflectance products from MODIS," *Remote Sens. Environ.* **83**(1–2), 135–148 (2002), http://dx.doi.org/10.1016/S0034-4257(02)00091-3.
10. C. L. Schaaf et al., "Retrieval of surface albedo from satellite sensors," in *Advances in Land Remote Sensing: System, Modeling, Inversion and Application*, S. Liang, Ed., pp. 219–243, Springer, Heidelberg, Germany (2008).
11. S. D. Miller et al., "A case for natural colour imagery from geostationary satellites, and an approximation for the GOES-R ABI," *Int. J. Remote Sens* **33**(13), 13 (2011), http://dx.doi.org/10.1080/01431161.
12. D. Hillger et al., "Synthetic advanced baseline imager true-color imagery," *J. Appl. Remote Sens.* **5**(1), 053520 (2011), http://dx.doi.org/10.1117/1.3576112.
13. W. R. Cotton et al., "RAMS 2001: current status and future direction," *Meteor. Atmos. Phys.* **82**(1–4), 5–29 (2003), http://dx.doi.org/10.1007/s00703-001-0584-9.
14. F. Mesinger et al., "North American regional reanalysis," *Bull. Amer. Meteor. Soc.* **87**(3), 343–360 (2006), http://dx.doi.org/10.1175/BAMS-87-3-343.
15. S. Moorthi, H.-L. Pan, and P. Caplan, "Changes to the 2001 NCEP operational MRF/AVN global analysis/forecast system," in *NWS Tech. Procedures Bull.*, Vol. 484, p. 14, National Weather Service (2001).
16. T. J. Greenwald, R. Hertenstein, and T. Vukicevic, "An all-weather observational operator for radiance data assimilation with mesoscale forecast models," *Mon. Wea. Rev.* **130**(7), 1882–1897 (2002), http://dx.doi.org/10.1175/1520-0493(2002)130<1882:AAWOOF>2.0.CO;2.
17. L. D. Grasso and T. Greenwald, "Analysis of 10.7 μm brightness temperatures of a simulated thunderstorm with two-moment microphysics," *Mon. Wea. Rev.* **132**(3), 815–825 (2004), http://dx.doi.org/10.1175/1520-0493(2004)132<0815:AOMBTO>2.0.CO;2.
18. L. D. Grasso et al., "Synthetic satellite imagery for current and future environmental satellites," *Int. J. Remote Sens.* **29**(15–16), 4373–4384 (2008), http://dx.doi.org/10.1080/01431160801891820.
19. K. F. Evans, "The spherical harmonics discrete ordinate method for three-dimensional atmospheric radiation transfer," *J. Atmos. Sci.* **55**(3), 429–446 (1998), http://dx.doi.org/10.1175/1520-0469(1998)055<0429:TSHDOM>2.0.CO;2.
20. D. L. Mitchell, "Parameterization of the Mie extinction and absorption coefficients for water clouds," *J. Atmos. Sci.* **57**(9), 1311–1326 (2000), http://dx.doi.org/10.1175/1520-0469(2000)057<1311:POTMEA>2.0.CO;2.
21. W. Lucht, C. B. Schaaf, and A.H. Strahler, "An algorithm for the retrieval of albedo from space using semiempirical BRDF models," *IEEE Trans. Geosci. Remote Sens.* **38**(2), 977–998 (2000), http://dx.doi.org/10.1109/36.841980.
22. C. L. B. Schaaf et al., "MODIS albedo and reflectance anisotropy products from aqua and terra," in *Land Remote Sensing and Global Environmental Change: NASA's Earth*

Observing System and the Science of ASTER and MODIS, Remote Sensing and Digital Image Processing Series, B. Ramachandran, C. Justice, and M. Abrams, Eds., Vol. 11, p. 973, Springer-Verlag, Heidelberg, Germany (2011).
23. M. O. Román et al., "The MODIS (Collection V005) BRDF/albedo product: assessment of spatial representativeness over forested landscapes," *Remote Sens. Environ.* **113**(11), 2476–2498 (2009), http://dx.doi.org/10.1016/j.rse.2009.07.009.
24. M. O. Román et al., "Assessing the coupling between surface albedo derived from MODIS and the fraction of diffuse skylight over spatially-characterized landscapes," *Remote Sens. Environ.* **114**(4), 738–760 (2010), http://dx.doi.org/10.1016/j.rse.2009.11.014.
25. J. Liu et al., "Validation of moderate resolution imaging spectroradiometer (MODIS) albedo retrieval algorithm: dependence of albedo on solar zenith angle," *J. Geophys. Res.* **114**(D1), D01106 (2009), http://dx.doi.org/10.1029/2008JD009969.
26. J. Salomon et al., "Validation of the MODIS bidirectional reflectance distribution function and albedo retrievals using combined observations from the aqua and terra platforms," *IEEE Trans. Geosci. Remote Sens.* **44**(6) (2006), http://dx.doi.org/10.1109/TGRS.2006.871564.
27. J. S. Reid et al., "A review of biomass burning emissions part III: intensive optical properties of biomass burning particles," *Atmos. Chem. Phys.* **5**(3), 827–849 (2005), http://dx.doi.org/10.5194/acp-5-827-2005.
28. A. J. Prata and I. F. Grant, "Determination of mass loading and plume heights of volcanic ash clouds from satellite data," CSIRO Atmospheric Research Technical Paper No. 48 (2001).
29. G. D. Rolph et al., "Description and verification of the NOAA smoke forecasting system: the 2007 fire season," *Weather Forecasting* **24**(2), 361–378 (2009), http://dx.doi.org/10.1175/2008WAF2222165.1.
30. E. M. Prins and W. P. Menzel, "Geostationary satellite detection of biomass burning in South America," *Int. J. Remote Sens.* **13**(15), 2783–2799 (1992), http://dx.doi.org/10.1080/01431169208904081.

Lewis Grasso received his BS in meteorology from Lyndon State College in 1985. Both his MS (1993) and PhD (1996) in atmospheric science were obtained from Colorado State University. His areas of interest include numerical modeling and satellite meteorology. His interests moved into the area of producing synthetic satellite imagery from numerical model output. For the past few years, he has been focused primarily on generating synthetic NPOESS VIIRS and GOES-R ABI imagery for a variety of weather and environmental events: severe storms, lake effect snow, hurricanes, and wildfires.

Donald W. Hillger earned a BS in physics (1973) from the University of Minnesota, and MS (1976) and PhD (1983) in atmospheric science from Colorado State University. He continued as a postdoctoral fellow and later as a research associate at the Cooperative Institute for Research in the Atmosphere at Colorado State University before joining the Regional and Mesoscale Meteorology branch of NOAA/NESDIS as a research meteorologist in 1987. He specializes in satellite meteorology from geostationary and polar-orbiting platforms, as well as satellite instrument calibration/validation, satellite data/image quality, and planning for advanced and future instrumentation. Current research emphasis includes analysis of multispectral and hyper-spectral imagery and the development of image products from those datasets.

Crystal Barker Schaaf received her PhD degree in geography from Boston University in 1994 and received both the SB and SM degrees in meteorology from the Massachusetts Institute of Technology in 1982. She has been a long-term research professor in the Center for Remote Sensing and Department of Geography and Environment at Boston University and has recently joined the faculty of the Department of Environment, Earth, and Ocean Sciences at the University of Massachusetts, Boston. She works on the development of operational products for the moderate resolution imaging spectroradiometer (MODIS) launched on board the Terra and Aqua satellite platforms as part of NASA's Earth Observing System (EOS). She is the MODIS science team member leading the global BRDF/Albedo effort. She is also a science team member for the Visible/Infrared Imager/Radiometer Suite on board the joint NOAA/

NASA NPOESS Preparatory Project (NPP) satellite (NPP is the precursor to the next generation of national meteorological satellites). Her current research interests include the modeling of reflectances and albedo from anisotropic surfaces and the use of remote sensing data to reconstruct and monitor the bidirectional reflectance characteristics of various land surfaces, including vegetation phenology and land surface change.

Zhuosen Wang received his BS in geography from Beijing Normal University, China (2003), and PhD (2011) in geography from Boston University. He has been a postdoctoral fellow in the Environment, Earth, and Ocean Sciences Department at the University of Massachusetts, Boston. His areas of interest include the modeling and evaluation of the anisotropic characteristics and albedo of the land surface during the snow-covered and dormant period, the land surface modeling, and the monitoring of the vegetation phenology using satellite data.

Renate Brummer received the equivalent of an MS in mathematics and physics from the Universität München, Munich, Germany, in 1981 and a PhD in meteorology and physical oceanography from the University of Miami, Florida, in 1986. Her areas of interest include mesoscale forecast modeling, satellite meteorology, and environmental education/outreach. She has been a CIRA employee since 1995 and has been working as project manager for different CIRA projects. During those years she managed the systems development team for the international school program GLOBE. She also managed the so-called FX-Net project, a meteorological forecaster workstation that provides the user interface and functionality of the AWIPS workstation (used by NWS forecasters) via the Internet. During the last two years, Renate worked as a project coordinator for CIRA's Regional and Mesoscale Meteorology branch.

Robert DeMaria received his BS in computer science from Colorado State University (2006). While a CSU student, Robert worked as a student hourly at CIRA. During this time he was responsible for performing data processing jobs and miscellaneous programming support tasks. During the fall of 2006, he was the teaching assistant for the senior level computer graphics course at CSU. In 2007, he joined CIRA as a research associate I.